Wave propagation on helices and hyperhelices: a fractal regression

By N. H. Fletcher[1], T. Tarnopolskaya[2] and F. R. de Hoog[2]

[1]Research School of Physical Sciences and Engineering,
Australian National University, Canberra 0200, Australia
[2]CSIRO Mathematical and Information Sciences,
GPO Box 664, Canberra 2601, Australia

A hyperhelix of order N is defined to be a self-similar object consisting of a thin elastic rod wound into a helix, which is itself wound into a larger helix, until this process has been repeated N times. Wave propagation on such a structure can be discussed in a hierarchical manner, ultimately in terms of the wavenumber k defining propagation on the elementary rod. It is found that the dispersion curve expressing the wave frequency ω as a function of the elementary wavenumber k on the rod making up the initial helix is also a fractal object, with all the macroscopically observable wave phenomena for a hyperhelix of arbitrarily large order being compressed into a small wavenumber range of width about $2R_2^{-1}\alpha$ centred on the value $k = R_1^{-1}$, where R_1 is the radius, α is the helical pitch angle of the smallest helix in the progression, and R_2 is the radius of the next-larger helix.

Keywords: vibrations; waves; helix; hyperhelix; spring

1. Introduction

This paper presents a description of wave propagation on rods, helices and hyperhelices—a term by which we mean helices coiled up into helices, coiled up into helices, etc.—in a self-similar regression that makes the hyperhelix a fractal object. Motivation for the study was initially a quite practical concern, with the behaviour of flexed elastic rods and foils (Tarnopolskaya *et al.* 1996), but the present extension to these complex geometrical objects derives from analogy with the string theory of elementary particles, in which hidden dimensions are coiled up invisibly within simple structures resembling strings or springs. It is, however, not claimed that the present discussion has any relevance to that abstract theoretical field. On a more practical scale, the vibrations of helices and hyperhelices are important at the molecular level in biological structures (Furois-Corbin *et al.* 1995), though again it is not clear that our present discussion has any direct relevance.

2. Helices

Wave propagation on a long thin rod is a classical subject, to which approximate solutions have been known for a long time (Love 1927). There are three different

types of waves possible: longitudinal compressive waves, L_0, with wave speed c^L_0; torsional waves, Ψ_0, with speed c_{Ψ_0}, and transverse waves, T_0, with speed c^T_0. (The significance of the subscript 0 will become apparent later.) There are two possible polarizations T_0 and T'_0 of the transverse waves, but their behaviour is identical. If ρ is the density, E the Young's modulus and G the shear modulus of the rod material, and if its cross-section is a solid circle of radius r, then these wave speeds are given, to a good approximation, by

$$c^L_0 = \left(\frac{E}{\rho}\right)^{1/2}, \qquad c_{\Psi_0} = \left(\frac{G}{\rho}\right)^{1/2}, \qquad c^T_0 = \omega^{1/2}\left(\frac{Er^2}{4\rho}\right)^{1/4}, \qquad (2.1)$$

where ω is the angular frequency of the vibration. The expression for c^T_0 applies only if the wavelength λ is very much greater than the rod radius r; in the contrary limit when $\lambda \ll r$, the bending waves become shear waves and $c^T_0 \to (G/\rho)^{1/2}$. If we define the wavenumber k to be $k = 2\pi/\lambda$ as usual, then the third of equations (2.1) applies only if $kr \ll 1$. More complicated and exact versions of each of these equations are known, but it would complicate the discussion unnecessarily to use these here.

(a) Wave modes at low wavenumber

The mechanics of a simple helical spring, made by uniform bending of such a rod, is of immense practical importance and has been the subject of considerable study. The static elastic properties of such springs, in the limit of infinitesimal distortions, have long been understood (Love 1927; Timoshenko & Goodier 1951). The basic restoring force for all ordinary displacements is derived from torsion of the elementary rod, with shear stresses playing a much smaller role. This simple situation is, however, greatly complicated when the distortions of the helix become appreciable compared with its diameter. Because our present discussion is restricted to the linear domain, it is not necessary to examine these complex and interesting problems here.

Wave propagation on helices has also received attention. Love, for example, cites works as early as those of Saint-Venant in 1843. An excellent treatment appropriate to our present purpose has been given by Wittrick (1966), who derives expressions for the propagation velocities V' and V of torsional and bending waves, respectively, along the rod from which the helix is made. These expressions, which are valid only when the wavelength is long compared with the helical radius, can be written as

$$V' = c_{\Psi_0}\left(\frac{r}{\sqrt{2}R_1}\right), \qquad V = c^L_0\left(\frac{r}{2R_1}\right), \qquad (2.2)$$

where r is the rod radius and R_1 is the radius of the helix. While these velocities are independent of the helical pitch angle $\alpha_1 = \tan^{-1}(h_1/2\pi R_1)$, where h_1 is the pitch of the helix, the exact specification of the direction of vibration of the two waves does depend upon this angle. If $\alpha_1 \to 0$, then the description becomes very simple. This is not a physically attainable configuration, but for most practical helices α_1 is small. Note that, unlike the case of bending-wave propagation along a straight rod, there is here no dispersion of bending waves, but this conclusion applies only if $\lambda \gg 2\pi R_1$, or equivalently if $k \ll R_1^{-1}$.

It is useful to have a mental image of these two types of waves on the helix, and this is provided in figure 1a. A wave of type Ψ_0 that is torsional when viewed at the
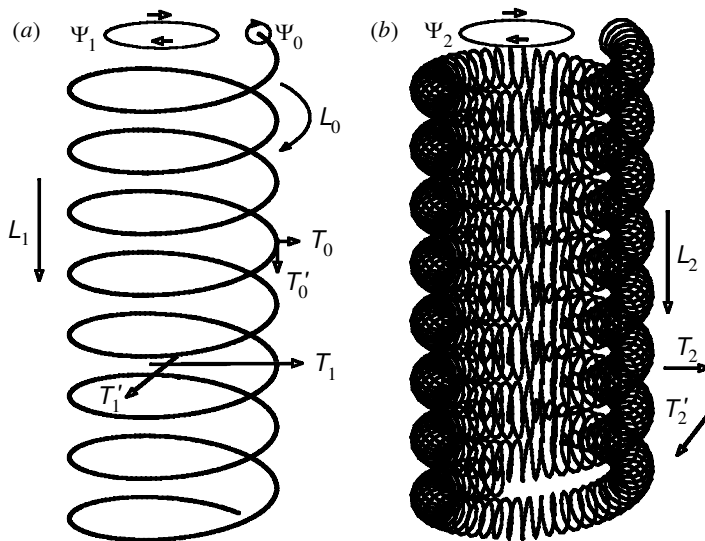
Figure 1. (a) A simple helix. The torsional, Ψ_0, longitudinal, L_0, and transverse, T_0 and T_0', motions at the level of the elementary curved rod are identified, as are their alternative descriptions as torsional, Ψ_1, longitudinal, L_1, and transverse, T_1 and T_1', modes of the first-order helix. (b) A hyperhelix of order 2, which might also be described as a superhelix. There is a similar hierarchy of macroscopic modes Ψ_2, L_2, T_2 and T_2' on this structure, as well as hidden microscopic modes of orders 1 and 0 on the elementary helix and the elementary rod.

level of the curved rod of the helix is actually an axially extensional mode, which is longitudinal for the helix as a whole and can thus be denoted by L_1. As is known from the theory of static strain in helical springs, longitudinal extension L_1 of zero wavenumber is in fact produced by torsional strain Ψ_0, so that the amplitudes are related by

$$T_0' = 4R_1\Psi_0. \tag{2.3}$$

Similarly, a long-wavelength transverse T_0 mode, which is flexural on the level of the rod and polarized in its plane of curvature, causes expansion or contraction of the turns of the helix in a varicose manner, and is torsional about the axis of the helix, so that it can be denoted by Ψ_1. Both these mode types are axially symmetric at the level of the helix.

Viewed at the level of the helix, the two wave propagation velocities in this limit $k \ll R_1^{-1}$ are

$$c_{L_1} \approx c_{\Psi_0}\left(\frac{r}{2R_1}\right)\sin\alpha_1, \qquad c_{\Psi_1} \approx c_{L_0}\left(\frac{r}{R_1\sqrt{2}}\right)\sin\alpha_1. \tag{2.4}$$

The macroscopic wavenumber k_{i_1} on the helix is given in each case by $k_{i_1} = \omega_i/c_{i_1}$, where i denotes the wave type. There must clearly also be modes that describe the transverse oscillation of the helix as a whole, which would be designated T_1, but the origin of these modes is not apparent from the analysis so far; they will form a major part of the discussion in § 2 c below.

(b) Wave coupling

A detailed study of the coupling between torsional and transverse modes on a helix has been published by Jiang *et al.* (1991). It is appropriate to present here a comparable analysis of the coupling between longitudinal and transverse modes, since it is these that will be our primary concern.

For a thin rod or radius r, material density ρ, Young's modulus E and uniform curvature κ, the wave equations developed by Love (1927) for displacements in the plane of curvature can be written in the form (Tarnopolskaya *et al.* 1999*a*)

$$\frac{\partial^2 u}{\partial t^2} = \frac{E}{\rho}\left(\frac{\partial^2 u}{\partial s^2} - \kappa\frac{\partial v}{\partial s}\right), \tag{2.5}$$

$$\frac{\partial^2 v}{\partial t^2} = -\frac{Er^2}{4\rho}\left(\frac{\partial^4 v}{\partial s^4} + 2\kappa^2\frac{\partial^2 v}{\partial s^2} + \kappa^4 v\right) + \frac{E\kappa}{\rho}\left(\frac{\partial u}{\partial s} - \kappa v\right), \tag{2.6}$$

where the tangential displacement has been written as $u(s)$ and the radial displacement as $v(s)$, and s measures tangential distance along the elementary rod. Clearly these reduce to the familiar equations for longitudinal and transverse waves on a straight rod when $\kappa = 0$. These equations apply to a good approximation to waves on a helix, provided the helical pitch angle α is small.

Longitudinal and transverse waves on the rod can be written in the form

$$u(s) = u\cos(k_1 x - \omega t + \phi), \qquad v(s) = v\cos(k_2 x - \omega t), \tag{2.7}$$

and it is clear from the form of (2.5) and (2.6) that wave coupling occurs only if $k_1 = k_2 = k$ and $\phi = \pi/2$. Substitution of (2.7) into (2.5) and (2.6) gives two solutions for the frequency ω. The solution of higher frequency gives, for $k \ll \kappa$,

$$\omega \approx \left[\frac{E}{\rho}\left(k^2 + \frac{r^2\kappa^4}{4}\right)\right]^{1/2}, \qquad \frac{u}{v} \approx \frac{4k}{r^2\kappa^3}. \tag{2.8}$$

The wave is essentially longitudinal, though with a transverse wave admixture, the magnitude of which depends upon the rod radius and thus its bending stiffness. The frequency for a given wavenumber k rises gradually from the normal longitudinal-wave frequency as the curvature is increased. This wave will not be considered further here.

The solution of lower frequency gives, for $k \ll \kappa$,

$$\omega \approx \left(\frac{E}{\rho}\right)^{1/2}\frac{r\kappa k}{2}, \qquad \frac{u}{v} \approx \frac{\kappa}{k} \tag{2.9}$$

and is of particular interest here. Although the wave is nominally transverse in terms of origin and frequency, for $k \ll \kappa$ the motion is predominantly longitudinal, and the relative magnitude of the longitudinal and transverse components is very nearly that required to eliminate the cross-term in equation (2.6). Precise cancellation does not, however, occur, and for increasing curvature the mode frequency rises approximately linearly with κ. This result has been verified in detail, both theoretically and experimentally, for the case of finite helices (Tarnopolskaya *et al.* 1999*b*). For $k \ll \kappa$ the mode shape is axially symmetric on the helix and can be termed 'varicose'.

The relation (2.9) suggests, and more detailed investigation confirms, that $\omega \approx 0$ and $u \approx v$ when $k \approx \kappa$. This surprising result will be seen later to correspond to simple sinuous motion of the helix as a whole.
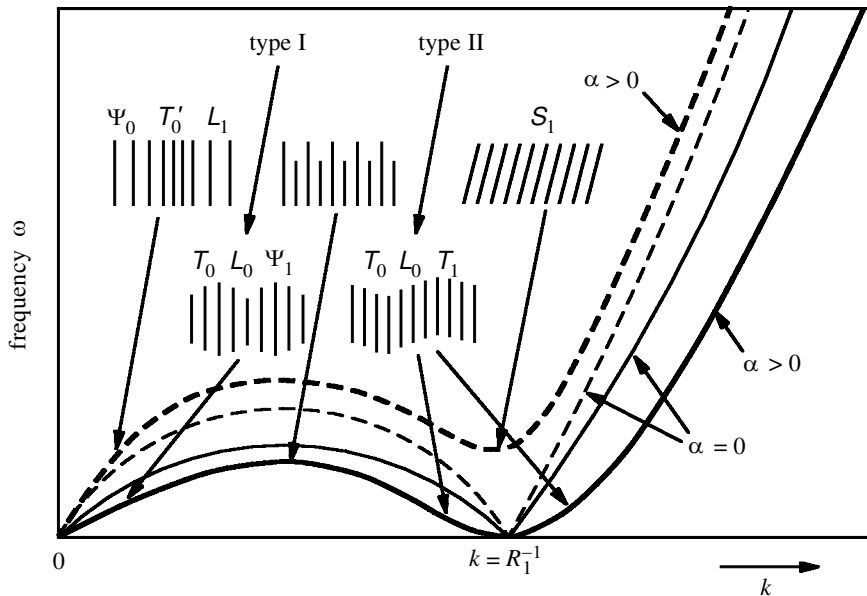
Figure 2. Qualitative dispersion curves for waves on a helical spring. The full curves refer to modes of type L_0 or Ψ_1 as $k \to 0$ but type T_0 or T_1 near $k = R_1^{-1}$; the broken curves refer to modes of type Ψ_0 or L_1 near $k = 0$ but of diametral shear type S_1 near $k = R_1^{-1}$. In each case the bold curve relates to the practical case $\alpha \neq 0$ and the light curve to the idealized case where $\alpha = 0$. Sketches show a cross-section of the helix for various values of k. Standing-wave modes of types I and II, as identified by Tarnopolskaya *et al.* (1999b), are also labelled. Dispersion curves are from the analysis of della Pietra & della Valle (1982).

(c) Higher wavenumbers

An extension to the theory of Wittrick was made by Kagawa (1968), who showed that when the calculations are extended to higher frequencies, the input impedance of a finite helix exhibits much more complex behaviour, with a generally low-pass frequency characteristic, followed at higher frequencies by a stop-band. His calculations of mechanical input impedance for longitudinal, L_1, and torsional, Ψ_1, vibrations of a finite spring led him to suggest that an infinite helix should also exhibit successive pass-bands and stop-bands for both these wave types. Our discussion below does not extend to frequencies where this phenomenon might appear, but is restricted to the band of lowest frequency.

Della Pietra & della Valle (1982) examined the axially symmetric vibrations of helical springs and showed that, for the longitudinal L_1 mode of a helix, the dispersion curve $\omega^L(k)$ rises from zero to a maximum near $k = 0.5R_1^{-1}$ and then falls to a minimum at $k = R_1^{-1}$, as shown by the broken curves of figure 2. The exact shape of the dispersion curve near $k = R_1^{-1}$ depends upon the value of the helical pitch angle α_1, the minimum being a sharp cusp at zero frequency if $\alpha_1 = 0$. For $k > R_1^{-1}$ the dispersion curve rises again without limit. The behaviour of $\omega_\Psi(k)$ for the Ψ_1 torsional mode is similar, except that the frequency falls to zero at $k = R_1^{-1}$ for all values of α_1, as shown by the two full curves of figure 2. For simplicity in what follows, we shall restrict discussion to cases in which the helical pitch angle α is small

enough that $\sin\alpha \approx \tan\alpha \approx \alpha$ and write α indifferently (without concern for minor differences) for either of these quantities.

The reasons for this behaviour can be seen when the displacement structure of the waves near this minimum is examined. Consider first the upper curve. Although there is strong coupling between transverse displacements, T'_0, parallel to the helical axis and torsional displacements, Ψ_0, on the elementary rod, it is sufficient, from the viewpoint of geometry, to consider only the former. If $\hat{r}$ is a unit vector in the radial direction on the helix and $\hat{s}$ and $\hat{z}$ similar unit vectors in the tangential and axial directions, then, for a wavenumber k, the displacement associated with T'_0 is $A\hat{z}\sin ks$. If $k \ll R_1^{-1}$, then this displacement is nearly constant over any helical turn, and the result is a simple longitudinal wave L_1 on the helix, with zero frequency at $k = 0$. The dispersion curve then rises with increasing k. For $k = R_1^{-1}$, however, there is a whole wavelength around each helical turn, and the displacement has the form of a shear of the helix about a diameter, as shown for the wave labelled S_1 in figure 2. If the helical pitch angle α_1 is zero, then there is no elastic strain associated with this simple rotation of the whole compressed helix, so the frequency becomes zero. For any non-zero helical angle, however, there is significant elastic strain, and the dispersion curve simply has a local minimum. This broadly explains the shape of the broken curves in figure 2.

The helix mode defined as Ψ_1 for small k, and derived from the elementary modes T_0 and L_0, has already been discussed. As shown in § 2 b, this mode, though nominally transverse, has a large longitudinal component, the magnitude of which is almost sufficient to cancel the effects of curvature. If $k \ll \kappa$, the result is an axially symmetric varicose mode on the helix.

In the case when $k = R_1^{-1}$, there is again just one wavelength of the disturbance around each helical turn, and energy is minimized if $u = v$ and, once again, $\phi = \pi/2$. For this choice of parameters, the motion defined by (2.7) is a simple bodily displacement of the whole helix parallel to the direction of the radius vector to the point $s = 0$. Because there is no associated elastic strain in the helix, the frequency is zero, whatever the value of the helical pitch angle α_1.

If $k = R_1^{-1}(1 - \delta)$ with $0 < |\delta| \ll 1$, then the direction of displacement of each helical turn differs by an angle δ from that of its nearest neighbour. The displacement itself therefore defines a helical wave with wavelength $2\pi/\delta$ turns of the physical helix and with the chirality determined by the sign of δ. This wave, labelled as T_1, is sketched near the point $k = R_1^{-1}$ on the full curve in figure 2. If two such circularly polarized co-propagating waves with elementary wavenumbers $R_1^{-1}(1 \pm \delta)$, and thus opposite chirality, are added, then the result is a plane polarized transverse wave with macroscopic wavelength $4\pi^2 R_1\alpha_1/\delta$. We might call this a sinuous mode. The macroscopic wavenumber k^{T_1} when this sinuous wave is viewed at the level of the helix is

$$k^{T_1} = \frac{k - R_1^{-1}}{2\pi\alpha_1}, \tag{2.10}$$

so that the zero for k^{T_1} is shifted to the frequency zero at $k = R_1^{-1}$ and its scale is changed by a factor $2\pi\alpha_1$.

If α_1 is non-zero, as it must be in physical reality, then the two modes T_1 and S_1 must be coupled to some extent, as in the bending of a thin solid rod. This does not destroy the precise frequency minimum in T_1 at $k = R_1^{-1}$, but makes the curve rise

parabolically rather than linearly away from this minimum, again as in the case of transverse wave dispersion on a thin rod.

We note also that at the maximum of the dispersion curve near $k = 0.5R_1^{-1}$ there is about one half wavelength of the fundamental disturbance on each turn of the helix. This means that the helical turns will be alternately expanded and contracted radially, as well as being displaced sideways, under the influence of the fundamental wave T_0, as shown in figure 2. Such a situation clearly leads to a large contribution to the strain energy, so that it is not surprising that the frequency reaches a maximum value.

Globally considered, the macroscopic behaviour near the minima of the dispersion curve is just what is to be expected from our qualitative practical experience of the small-amplitude vibration of long thin helical springs, such as those encountered in hardware shops. At a macroscopic level, the helical structure is irrelevant, and the helix behaves like a simple straight rod of very small stiffness, provided all distortions are kept small. Longitudinal and transverse standing waves constructed from L_1 and T_1 behave like simple vibrations with small values of the macroscopic wavenumber kT_1, though at a deeper level they are derived from L_0, T_0 and Ψ_0 waves centred around the wavenumber $k = R_1^{-1}$. These statements apply, however, only for waves with amplitudes that are small compared with their macroscopic wavelength. Helices may well exhibit peculiar static and dynamic properties under conditions of larger elastic strain.

In a sequence of previous papers (Tarnopolskaya *et al.* 1996, 1999*a*, *b*), we treated this whole problem in a rather different way, which is, however, complementary to the present discussion. (Note that, in those papers, the symbol α had a meaning different from that assigned here.) The approach was to begin from the equations for a slightly curved rod of finite length, clamped at both ends, and then follow the development of the modes as the curvature was increased to convert the rod into a helix. Only the case in which the helical pitch angle $\alpha_1 = 0$ was considered explicitly. The mode transitions and couplings between the various zeroth-order modes can be appreciated in detail, and the conclusions are compatible with those of the present propagation approach in the limit in which the number of turns on the helix becomes very large. Two different mode types were identified in this limit. One, termed type I, is equivalent to a standing wave formed from superposition of two counter-propagating Ψ_1 modes with $k \ll R_1^{-1}$, and has a varicose shape. The other, termed type II, is a superposition of two counter-propagating T_1 modes with $k \approx R_1^{-1}$, and has a sinuous superhelical shape. The precise boundary and excitation conditions for a finite helix may cause a coupling between T_1 and T_1' modes to give plane polarized vibrations. Two orthogonal polarizations of each type II mode are then possible.

In this standing-wave model, the modes are ordered in frequency according to a simple algebraic rule,

$$\omega_n^{\mathrm{I}} \approx n^{1/2}\omega_0, \qquad \omega_n^{\mathrm{II}} \approx (2n)^{1/2}\omega_0, \tag{2.11}$$

the type II mode frequencies being essentially twofold degenerate for a sufficiently long helix. The physical origin of this result was initially obscure. It can now be seen to arise from interleaving of Ψ_1 and pairs of T_1 modes from the vicinity of the two zeros of the dispersion curve; a horizontal line drawn in figure 2 would intersect the dispersion curve, shown as a full line, in three places.

3. Hyperhelices

We can now extend this analysis to a yet more complex structure that we shall term a hyperhelix. A hyperhelix of order n is constructed by curving to helical form a hyperhelix of order $n-1$. A simple rod can be defined to be a hyperhelix of order 0, so that an ordinary helix is a hyperhelix of order 1. This convention explains the use of numbers in the description of modes in the previous sections. With this definition, a hyperhelix is essentially a fractal object, with similar structure at all scales, though in practice this regression terminates when order 0 is reached. If the pitch angles α_n and size ratios R_n/R_{n+1} are taken to be constant throughout the regression, then the Hausdorff (or capacity) dimension D for such a structure can be readily calculated (see, for example, Baker & Gollub 1996) and has the value

$$D = \frac{\log(\alpha R_n/R_{n+1})}{\log(R_n/R_{n+1})}. \tag{3.1}$$

Since geometrical considerations forbidding overlap require that $R_n/\pi R_{n+1} < \alpha < 1$, and since $R_n \ll R_{n+1}$, the dimension D lies in the range $1 < D < 2$ and is typically towards the lower end of this range.

Consider a hyperhelix of order 2, consisting of a helix of radius R_1 wrapped into a superhelix of radius R_2, where $R_2 \gg R_1 \gg r$, as shown in figure 1b. In the limit as $k \to 0$, the only available first-order modes are the longitudinal and torsional modes L_1 and Ψ_1. These modes are, however, internal to the first-order hyperhelix, and do not have any macroscopic manifestation at the second-order level.

For detectable macroscopic modes, the region near $k = R_1^{-1}$ must be invoked. Exactly at $k = R_1^{-1}$ there are two possibilities. Either the displacement of the first-order helix is parallel to the axis of the second-order hyperhelix, giving a simple axial displacement, denoted by L_2, or else it is normal to this axis, giving a radial dilatation Ψ_2 of the hyperhelix, as shown in figure 1b. In either case the frequency is zero, for the reasons discussed in relation to the simple helix.

If we now consider a neighbouring point in wavenumber space for which $k = (1+\delta)R_1^{-1}$, then the situation becomes much more complex. The reason for this is that the displacement of the first-order helix is superhelical, as discussed in §2c above, so that the resulting displacement of the turns of the second-order hyperhelix varies between radial and axial around a single hyperhelical turn. If we denote the radial direction in the hyperhelix by $\hat{\boldsymbol{r}}_1$, the tangential direction by $\hat{\boldsymbol{s}}_1$, and the axial direction by $\hat{\boldsymbol{z}}_1$, then, by analogy with (2.7), the displacement at tangential position s is

$$A\hat{\boldsymbol{r}}_1 \cos ks + A\hat{\boldsymbol{z}}_1 \sin ks - A\hat{\boldsymbol{s}}_1 \sin ks. \tag{3.2}$$

This is a complex distortion—essentially equivalent to a superposition of a sinuous wave and an equal shear wave of type S_1—with a considerable amount of elastic strain energy. As with the case of superhelical waves on a simple helix, however, the situation simplifies itself by the coupling of a co-propagating wave of equal amplitude and with wavenumber $(1-\delta)R_1^{-1}$, corresponding to the same macroscopic wavenumber k_1 but opposite chirality. This superposition cancels the axial term $A\hat{\boldsymbol{z}}_1 \sin ks$ and leaves a simple circularly polarized wave on the hyperhelix.

When considered in terms of the visible macroscopic waves involved, the behaviour of a hyperhelix of order 2 is therefore very similar to that of a simple helix of order 1.

If we denote the macroscopic wavenumber on the simple helix by k_1, then the wave frequency ω is zero when $k_1 = 0$, which itself corresponds to the value $k = R_1^{-1}$. The macroscopic motion under these conditions consists simply of torsional and longitudinal waves Ψ_2 and ${}^L{}_2$ of infinite wavelength on the hyperhelix.

If the elementary wavenumber k is increased slightly above the value R_1^{-1}, then the geometry of the hyperhelix imposes a coupling to another elementary wave with k just less than R_1^{-1}. When $k = R_1^{-1} \pm R_2^{-1}$, the frequency of this pair of coupled waves again falls to zero, corresponding to a simple transverse displacement of the hyperhelix with zero macroscopic wavenumber. If we denote the macroscopic wavenumber of transverse waves on the hyperhelix by k^{T_2}, then, by analogy with (2.10),

$$
k^{T_2} = \frac{k^{T_1} - R_2^{-1}}{2\pi\alpha_2}
$$
$$
= \frac{k - R_1^{-1}}{2\pi\alpha_1\alpha_2} - \frac{R_2^{-1}}{2\pi\alpha_2}, \tag{3.3}
$$

where α_2 is the macroscopic pitch angle of the hyperhelix and α_1 that of the first-order helix. Since, under our assumptions, α_1 and α_2 are both very small angles, it follows that all the macroscopic behaviour of the hyperhelix is compressed into a very small range of order $R_2^{-1}\alpha_1$ of the elementary wavenumber k centred around $k = R_1^{-1}$.

This situation is illustrated in figure 3, which shows qualitatively the progression of the dispersion curve through three orders of helix. Near each minimum in the curve for order n, the curve for order $n + 1$ splits, corresponding to circularly polarized (hyperhelical) waves of opposite chiralities, and these two waves then combine to produce a simple plane-polarized wave on the hyperhelix. These wave couplings are indicated by bracketing lines. Clearly the figure, which is only qualitative, cannot indicate all this detail, but it does summarize the essence of our conclusions. There is, indeed, no single-valued dispersion curve for elementary waves on a hyperhelix. Instead, coupling between waves of opposite chirality gives the effective dispersion curve a fractal structure. The capacity dimension d of the set of points for which the frequency is zero can be readily calculated, the result being

$$
d = -\frac{\log 2}{\log(R_n\alpha/R_{n+1})}. \tag{3.4}
$$

Since, as noted previously, $R_n/\pi R_{n+1} < \alpha \ll 1$, this dimension is confined within the approximate limits $\log 2/\log M < d < \log 2/2\log M$, where M is the scaling ratio R_{n+1}/R_n and is a large number.

4. Conclusions

The class of hyperhelices presents many interesting features when their vibrational behaviour is examined. The hyperhelices themselves have a fractal structure, and this is reflected in the dispersion curves for waves travelling along them, which similarly have fractal attributes. It is interesting, however, that none of these subtle features are observed when the vibrational properties of a macroscopic hyperhelix are studied. Instead, it behaves as a simple elastic object very similar to a structureless flexible rod. It is only when means are found to examine vibrational motions at a finer level that interesting and unusual properties emerge.
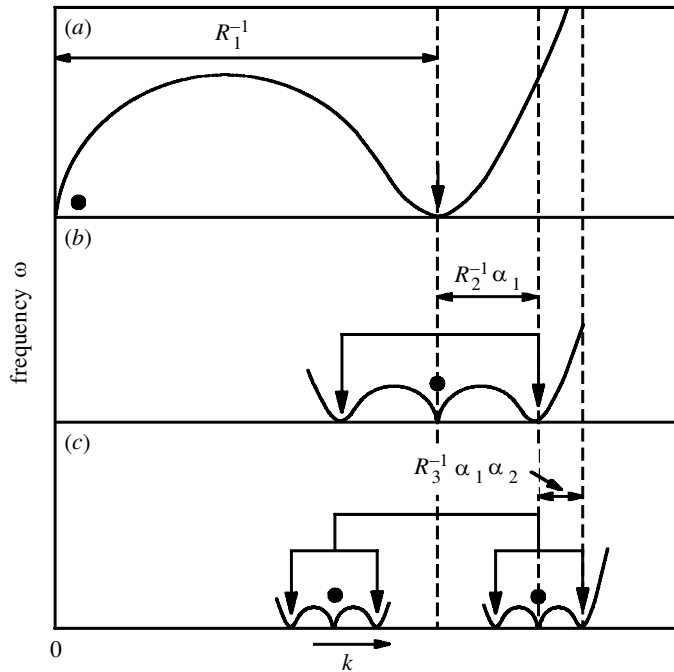
Figure 3. Simplified qualitative dispersion curves for hyperhelices of order (*a*) 1, (*b*) 2 and (*c*) 3. Only the lower branch of the curve is shown. For clarity, the relative magnitudes of successive steps R_n^{-1} have been made much more nearly equal than they would be in practice, so that the fractal region around $k = R_1^{-1}$ is greatly expanded in size. Heavy arrows indicate wavenumbers that are coupled to produce sinuous behaviour, and dark circles those that lead to varicose behaviour.

The discussion shows that the entire macroscopic transverse vibrational behaviour of a hyperhelix of order N is contained within the elementary wavenumber region

$$R_1^{-1} \pm \sum_{n=2}^{N} R_n^{-1} \prod_{m=1}^{N-1} \alpha_m. \tag{4.1}$$

For values of the elementary wavenumber k lying outside this domain, the wave behaviour is contained invisibly within hyperhelices of lower order. Thus, not only is the real-space geometry of a hyperhelix fractal, but so also are both the dispersion curves and the sub-universes of microscopic behaviour.

In this development we have begun from a small but not infinitesimal rod radius r, and each stage of helix construction has increased the helical radius R_n by at least a factor of 10, since we required that $R_n \gg R_{n-1}$. The final hyperhelix of large order N will, therefore, be an object of truly cosmic proportions. It is perhaps more useful to consider the final hyperhelical R_N to be of a comfortably finite size, so that the hyperhelical radii for smaller values of n rapidly become infinitesimal. Under this assumption, the wavenumber region defined by (4.1) encompasses a range of wavelengths for transverse, longitudinal and torsional vibrations of the hyperhelix that extends from the length of the hyperhelix down to a length comparable with the hyperhelical diameter. All other modes for smaller and larger values of k are hidden within the structure of the hyperhelix and are not visible on a macroscopic scale. If

the initial rod radius r is infinitesimal and the value of N approaches infinity, then the overall behaviour of the hyperhelix is truly fractal.

Finally, a comment should be made about the 'reality' of the fractal dispersion curves sketched in figure 3. While it is true that a macroscopic transverse wave on a hyperhelix is made up from a combination of co-propagating waves of different wavenumber, in much the same way as an ordinary square wave is made up of a super-position of co-propagating harmonic waves, the analogy is not precise. In ordinary wave propagation the component waves are truly independent and can propagate individually or in combination. In the helical and hyperhelical cases, the differential equations describing the waves are all strongly coupled, and the propagation of individual waves is not possible; only those combinations we have identified that lead to macroscopically simple waveforms are allowed. The only exception to this statement occurs for very large wavenumbers, $k \gg R_1^{-1}$, when the coupling tends to zero and waves of very short wavelength can propagate on the elementary rod from which the whole hyperhelix is constructed.

References

Baker, G. L. & Gollub, J. P. 1996 *Chaotic dynamics*, 2nd edn, pp. 110–114. Cambridge University Press.

della Pietra, L. & della Valle, S. 1982 On the dynamic behaviour of axially excited helical springs. *Meccanica* **17**, 31–43.

Furois-Corbin, S., Smith, J. C. & Lavery, R. 1995 Low-frequency vibrations in α-helices: helicoidal analysis of polyalanine and deoxymyoglobin molecular dynamics trajectories. *Biopolymers* **35**, 555–571.

Jiang, W., Jones, W. K., Wang, T. L. & Wu, K. H. 1991 Free vibration of helical springs. *Trans. ASME* **58**, 222–228.

Kagawa, Y. 1968 On the dynamical properties of helical springs of finite length with small pitch. *J. Sound Vib.* **8**, 1–15.

Love, A. E. H. 1927 *A treatise on the mathematical theory of elasticity*, 4th edn, pp. 414–431. Cambridge University Press.

Tarnopolskaya, T., de Hoog, F., Fletcher, N. H. & Thwaites, S. 1996 Asymptotic analysis of the free in-plane vibrations of beams with arbitrarily varying curvature and cross-section. *J. Sound Vib.* **196**, 659–680.

Tarnopolskaya, T., de Hoog, F. & Fletcher, N. H. 1999*a* Low-frequency mode transition in the free in-plane vibration of curved beams. *J. Sound Vib.* **228**, 69–90.

Tarnopolskaya, T., de Hoog, F. R., Tarnopolsky, A. & Fletcher, N. H. 1999*b* Vibration of beams and helices with arbitrarily large uniform curvature. *J. Sound Vib.* **228**, 305–332.

Timoshenko, S. & Goodier, J. N. 1951 *Theory of elasticity*, pp. 391–398. New York: McGraw-Hill.

Wittrick, W. H. 1966 On elastic wave propagation in helical springs. *Int. J. Mech. Sci.* **8**, 25–47.